Attractive forces on hard and soft colloidal objects located close to the surface of an acoustic-thickness shear resonator

Arne Langhoff and Diethelm Johannsmann[*]
Institute of Physical Chemistry, Clausthal University of Technology, 38678 Clausthal-Zellerfeld, Germany
(Received 16 May 2012; revised manuscript received 19 April 2013; published 2 July 2013)

Colloidal particles located close to the surface of an acoustic thickness shear resonator feel an attractive steady force, which is induced by the high-frequency tangential motion of the resonator surface. The range of the force is about half the penetration depth of the transverse viscous wave, that is, half of the thickness of the Stokes boundary layer. For an oscillation amplitude of 10 nm and a particle radius of 100 nm, the depth of attractive potential well corresponds to about 3 times the thermal energy, k_BT. The force therefore suffices to overcome Brownian motion.

DOI: 10.1103/PhysRevE.88.013001 PACS number(s): 47.57.J−, 47.11.Fg, 43.25.+y, 87.50.Y−

I. INTRODUCTION

Steady forces originating from oscillatory motions have been known since the late 19th century, when Reynolds described how and why dust particles migrate to the nodes of a standing acoustic wave [1]. Such steady forces also occur in the context of turbulence, where they are termed "Reynolds forces" [2]. Acoustophoresis, as the phenomenon is called in a technical context, can be used to pump liquids on small scales [3,4], to manipulate particles in a liquid without touching them [5,6], to separate different types of particles [7], and for biosensing [8]. A further field of application is medical ultrasound [9]. Making use of the Reynolds stress, one can remotely exert a static force onto a tissue. On a more mundane level, acoustically generated steady forces play a role in ultrasonic cleaning [10,11] and acoustic deagglomeration of particulate aggregates [12]. Recent reviews on the underlying theory are provided in Refs. [13,14], and [15]. With regard to microfluidics, the principles and current applications of acoustofluidics are summarized in a series of tutorial papers in *Lab on a Chip* [16].

The work reported below is concerned with a special geometry, namely nanoscopic particles located close to a solid surface, which undergoes a tangential oscillation. Such a surface emits a transverse viscous wave. In a sensing context, such waves are also called acoustic shear waves. Importantly, transverse viscous waves do not propagate in liquids. The penetration depth, δ, is given as $\delta = (2\eta/(\rho\omega))^{1/2}$ with η the viscosity, ρ the density, and ω the angular frequency. Inserting a frequency of 5 MHz (typical for a quartz crystal microbalance, see below) and the viscosity and density of water, one finds a penetration depth of 250 nm. The force described below is a phenomenon strictly limited to the boundary layer near the surface (also called Stokes layer). In the following, we use the terms "depth of penetration of the transverse viscous wave" and "thickness of the boundary layer" synonymously.

Colloidal particles close to a solid surface are of considerable relevance in acoustic sensing. The calculations below were motivated by experiments undertaken with a quartz crystal microbalance (QCM) [17,18]. The QCM is mostly known as an acoustic sensor [19]. It is a quartz plate with a thickness of a few hundred micrometers, which is piezoelectrically excited to undergo a thickness-shear vibration. The resonance is exceptionally sharp and shifts of the resonance frequency therefore can be determined with good precision (<0.1 ppm). The adsorption of single layers of proteins is readily evidenced from the adsorption-induced frequency shift. One of the problems of QCM-based sensing is the lack of specificity, that is, the difficulty in differentiating between different types of adsorbates. Edvardsson *et al.* [17] as well as Heitmann *et al.* [18] addressed this problem by running the sensor at an exceptionally large amplitude. They applied driving voltages of 10 V and above, which corresponds to amplitudes of oscillation at the resonator surface of tens of nanometers. The line of reasoning was that some kinds of analytes (Edvardsson and Heitmann were concerned with particles and biological cells, respectively) might be affected in their behavior by the high amplitude, while others might not. Both groups find adsorption to be prevented when the drive level is chosen high enough. Heitmann *et al.* find differences between different types of cells: For some cells the effect is stronger than for others and the approach might therefore serve to differentiate between cells.

Different ways by which a high-amplitude oscillation might affect the adsorption process come to mind. First, the effect might be genuinely mechanical. The bond between the particles and surface might be too weak to sustain the stress induced by the periodic vibration. This would imply that the particles can be shaken off after they have adsorbed. Such detachment events are reported in Ref. [20]. The authors of Ref. [17], on the other hand, emphasize that adsorption was irreversible, once it had occurred. Particles were prevented from adsorption only if the high-amplitude oscillation was kept on over the entire duration of the experiment. Once they had adsorbed, they stayed on the surface no matter how high the amplitude was ramped. A second mechanism by which particles might be prevented from adsorbing is a tangential steady flow, induced by the flexural contributions to the resonator's vibration [21]. While the resonator surface mostly moves in the tangential direction, there also is a normal component, which arises because the amplitude of oscillation

[*]Corresponding author: johannsmann@pc.tu-clausthal.de

is large in the center and decays towards the edge ("energy trapping"). A combined tangential and normal movement of a planar surface induces a tangential flow, as calculated by Wang and Drachman [22] and more recently discussed by Sadhal [23]. This flow can be readily observed with a video camera. We will discuss this flow and its consequences for particle adsorption separately [24]. A third type of steady force arises because particles and nanodroplets themselves distort the transverse viscous wave. This third mechanism is the focus of the current work. Pure transverse viscous waves do not produce steady forces because the direction of flow and the gradient direction are perpendicular. However, if the transverse flow is distorted by a particle, a steady force appears. The detailed calculation shows that this force cannot explain the experiments reported in Refs. [17] and [18] because it is directed *towards* the surface. Still, its occurrence has not been reported before and the force definitely is of relevance to acoustic sensing.

Steady forces between particles or bubbles and a tangentially vibrating surface were also reported in the context of experiments under conditions of microgravity [25–27]. Such forces initiate a convective flow, which may disturb the experiment (often crystallization). The vibration of the cell walls is caused by the so-called g-jitter. The configuration underlying these observations is more complicated than what is discussed below. The effects observed are not necessarily boundary layer effects; at least they are not portrayed as such in the literature. Also, the particles or bubbles are not small in the sense that they follow the motion of the background fluid. Both repulsive and attractive forces are observed. Contrasting to the results reported below, the steady force depends on the density mismatch between the object (particle or bubble) and the fluid. While there clearly is a connection between this work and Refs. [25–27], our results should not be directly applied to the configuration discussed there.

The paper is structured as follows. In Sec. II we elaborate on why particles located inside a Stokes layer are peculiar and why the steady force onto these particles cannot be calculated in the frame of Gor'kov theory [28]. This is a consequence of the viscous coupling between the particle and the source of excitation (the vibrating surface). In Sec. III, we describe a numerical calculation of the steady force onto hard and soft particles located inside the boundary layer. The calculation makes use of the finite-element method. An attractive force is found. Its range is half the thickness of the boundary layer and the dependence of force on distance is about exponential. The calculation is extended to nanodroplets, which experience a static deformation. In Sec. IV we show that the numerical result is well approximated by an analytical relation, derived by assuming that, first, the particle's internal deformation can be neglected; that, second, the particle mostly follows the motion of the background fluid; and that, third, the body force onto the particle is larger than the contact force exerted by the adjacent fluid. This approximation leads to a simple estimate for the strength of the force as a function of particle size and distance to the surface. Section V discusses a side aspect, which is the existence of a surface term occuring when there are discontinuities in density. Section VI concludes.

II. VISCOUS COUPLING BETWEEN THE PARTICLE AND TANGENTIALLY VIBRATING SURFACE

To start, we comment on assumptions and approximations. We assume the fluid to be incompressible. This is appropriate because the wavelength of conventional ultrasound (compressional waves) is around $\lambda = 300\ \mu$m in water at 5 MHz, whereas the thickness of the boundary layer is around $\delta = 250$ nm. Since $\lambda \gg \delta$, we can approximate λ as infinite, which amounts to incompressibility. Because the medium is incompressible, all steady flows originating from finite compressibility [29] vanish here.

We invoke a second approximation throughout all of this paper, which is that the amplitude is small enough for perturbation theory to be applicable [30]. We first calculate the flow field at the resonance frequency of the sensor, solving the *linear* problem of hydrodynamics with the given boundary conditions. Within the linear theory, particles can be allowed to be viscoelastic. The nonlinear form of the Navier-Stokes equation does not apply to viscoelastic solids, but the linearized form does. In a second step, we calculate the source term driving the steady flow. The source term is the advected momentum in the Navier-Stokes equation. This force drives a second-order, steady flow, the pattern of which (in a third step) is calculated by again using linear hydrodynamics. The steady velocity of the particle is converted to a force onto the particle by multiplying the velocity and with the particle's drag coefficient. The latter is also calculated from the linear model (see Sec. III). Note: This force is to be understood as an equivalent force, which would lead to the steady velocity as calculated in step 2 if the ambient liquid was quiescent (which it is not in experiment). It differs from the time-averaged advected momentum integrated over the particle volume.

The classical theory of acoustophoresis (following Gor'kov) treats particles in an *inviscid* fluid [28,29,31]. The formalism makes use of the fact that there are no steady bulk forces in an inviscid liquid far from the particle. Following Gor'kov, the force onto the particle is calculated from the particle's scattering amplitude [Fig. 1(a)]. The scattering amplitude must be evaluated in the far-field region because viscous effects are significant near the particle surface. There is a narrow layer close the particle surface (the Stokes layer), inside which the flow field deviates from inviscid flow in order to accommodate for the no-slip condition at the surface [32]. Gor'kov theory is *not* applicable to a particle close to a vibrating surface because the movement is excited across a viscous fluid [Fig. 1(b)]. Coupling to the source occurs through the near field. Excitation by viscous coupling has the interesting consequence that the particle rotates periodically, while rotation is negligible for a particle embedded in an inviscid fluid. The flow in the inviscid fluid is irrotational and therefore does not exert a torque onto the particle. Rotation is an essential element of the mechanism producing a steady force, as shown in Sec. IV.

III. NUMERICAL RESULTS OBTAINED BY THE FINITE-ELEMENT METHOD

In order to analyze the problem numerically, we have used the incompressible Navier-Stokes module supplied by

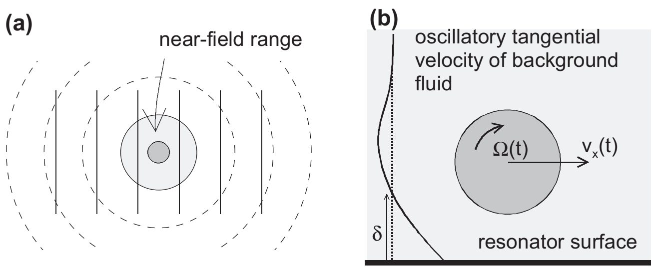

FIG. 1. (a) In the standard theory of acoustophoresis a particle is assumed to be immersed in an inviscid fluid and subjected to convential ultrasound (compressional waves). In the far field, the fluid is inviscid. The force onto the particle is calculated by integrating the stress over a surface located in the far field. The integral is related to the scattering amplitude. (b) The geometry under consideration here differs. The particle is located close a solid surface undergoing tangential oscillation. The surface emits an transverse viscous wave, which decays within a few hundred nanometers. The particle is located inside this boundary layer (Stokes layer). It undergoes a tangential translation with velocity $v_x(t)$ and a rotation with a rotational velocity $\Omega(t)$ at the same time. The particle's motion is excited by viscous coupling to the surface. There is no surface entirely located in the far field, which could serve as a surface of integration as in panel (a). An important consequence of the viscous coupling is the particle's periodic rotation. No such rotation occurs in standard acoustophoresis because the flow in an inviscid fluid is irrotational.

COMSOL (COMSOL GmbH, Göttingen, Germany). Unfortunately, this particular module only works in two dimensions. The calculations therefore describe cylinders rather than spheres, but they can still serve to demonstrate certain general features which should hold irrespective of particle shape. There are more advanced software packages for computational fluid mechanics on the market. The calculation of the steady force [to second order in $\mathbf{v}_u$, see Eq. (2)] can be added onto such calculations with moderate effort.

For this particular calculation we have modified an existing code described in Ref. [33] and Ref. [34], which predicts the MHz fluid flow at the surface of a quartz crystal microbalance. The software solves the Navier-Stokes problem in two dimensions. Importantly, the oscillation amplitude, $u_{q,0}$, was chosen small enough (0.01 nm) to ensure that the nonlinear term in the Navier-Stokes equation is negligible. Under such conditions, the software in effect solves the *linearized* Navier-Stokes problem, namely the equation

$$i\omega\rho v(\mathbf{r}) = -\eta\nabla^2 v(\mathbf{r}) + \nabla p(\mathbf{r}), \qquad (1)$$

where v is the velocity, ρ is the density, η is the viscosity, and p is the pressure. The software accounts for elastic stresses by a complex viscosity of the form $\eta' - i\eta''$. It computes a complex velocity field, $\mathbf{v}_{u,0}(\mathbf{r})$, which is the amplitude of the unsteady first-order flow as a function of position.

Once the linearized problem is solved, the solution can be scaled to any other amplitude. For comparison with experiment, it was scaled to $u_{q,0} = 10$ nm here. The index q (for quartz) denotes the resonator surface. Of course, this solution at $u_{q,0} = 10$ nm is the *first-order solution*. At an oscillation amplitude of 10 nm, the nonlinear term in the Navier-Stokes equation is not negligible, as evidenced by the occurrence of steady flows. The first-order solution is the starting point for a perturbation analysis, which predicts the steady flow.

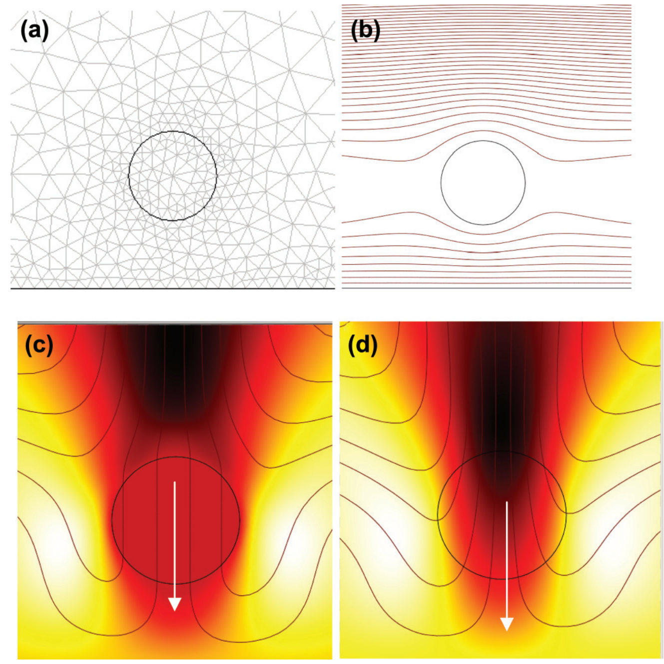

FIG. 2. (Color online) Geometry underlying the FEM calculation and raw outputs. A rigid sphere with radius $R = 100$ nm is located at a variable distance from the resonator surface (at the bottom). The surface oscillates tangentially with a frequency of 5 MHz. Panel (b) shows the stream lines of the first-order velocity field at 5 MHz. Panel (c) shows the streamlines of the steady, second-order flow driven by the steady force. In Panel (d), the rigid particle has been replaced by a droplet with a viscosity of twice the viscosity of the ambient liquid. In this case, there is deformation as well as translation. Colors (online version) and gray values (print version) encode the vertical component of the motion, where bright corresponds to upward motion. As indicated by the arrows, the particle moves downwards.

Figure 2(a) shows the geometry and the mesh. Only the portion of the simulation cell containing the particle is displayed. The particle radius was $R = 100$ nm, while the cell was 2 μm wide and 2 μm high. The height of the cell much exceeds the thickness of the Stokes layer. The cell boundary at the top was a wall at rest with a no-slip condition. The bottom of the cell is the resonator surface. It was assigned a no-slip condition with a tangential velocity of $v_{q,0} = i\omega u_{q,0}$. Periodic boundary conditions were applied to the right and to the left. Figure 2(b) depicts the streamlines of the first-order, unsteady flow as derived by solving the linearized problem. The viscosity of the liquid was 1 mPa s. The densities of the particle and the liquid were 1 g/cm^3. By choosing the density to be constant in space, we avoided the complications arising from the fact that the gradient in the Navier-Stokes equation applies to the product of density and velocity (Sec. V).

The steady force density (with index S) was calculated (to second order in $\mathbf{v}$) from the unsteady solution to the linear problem, $\mathbf{v}_{u,0}(\mathbf{r})$, as

$$\begin{aligned}\mathbf{f}_S(\mathbf{r}) &= -\langle(\mathbf{v}_u(\mathbf{r},t)\cdot\nabla)\,\rho\mathbf{v}_u(\mathbf{r},t)\rangle\\ &= -\frac{\rho}{2}\mathrm{Re}\left((\mathbf{v}_{u,0}(\mathbf{r})\cdot\nabla)\,\mathbf{v}^*_{u,0}(\mathbf{r})\right).\end{aligned} \qquad (2)$$

Angle brackets denote the time average, the star indicates the complex conjugate, and the index 0 denotes a complex amplitude. The force density as calculated with Eq. (2) was inserted as a body force into a second FEM calculation, which employs the same geometry and the same mesh as the first one. The second FEM calculation (at $\omega = 0$) differs from the first one (at frequency ω) in that it has the resonator surface at rest. The second calculation yields the steady second-order velocity field $\mathbf{v}_s(\mathbf{r})$. The stationary flow field derived in the second FEM calculation is shown in Figs. 2(c) and 2(d). The flow pattern displays the expected convection rolls. The particle moves downward. For the calculation shown in Fig. 2(c), the particle was assigned a storage modulus of $G' = 30$ GPa and vanishing loss modulus ($G'' = 0$). For all practical purposes, this amounts to a rigid object. Figure 2(d) shows the steady flow field obtained for a drop with a viscosity equal to twice the viscosity of the ambient liquid. The velocity is constant inside the rigid particle [Fig. 2(c)], while there is deformation for the droplet [Fig. 2(d)].

These calculations were repeated for various distances between the particle and the surface. Fig. 3(a) displays the velocity of the solid particle [cf. Fig. 2(c)], v_P, versus distance, z_q, where the distance is measured from the resonator surface to the lower edge of the particle. z_q is to be distinguished from the distance to the center of the particle [called z in Eq. (8)]. $|v_P|$ has a maximum at $z_q \approx R$. For particles located far away from the surface, the steady velocity eventually goes to zero because the decaying transverse viscous wave does not reach to these particles. For particles located just above the resonator surface, the streaming velocity also is small because of the strong hydrodynamic coupling between the particle and the surface (that is, the large friction coefficient, see below).

In order to assess the strength of this effect, we convert the steady velocity to a potential, which we then compare to the thermal energy, k_BT. The potential is calculated as an integral of the equivalent force, which would lead to the exact same steady velocity as displayed in Fig. 2(c) if the ambient liquid was quiescent. This equivalent force is not the same as the time-averaged advected momentum averaged over the particle volume because the neighboring fluid also exerts a force. The particle is driven towards the resonator surface by, first, the advected momentum integrated over its volume and, second, the drag exerted by the surrounding fluid (which also is in steady motion). The product of velocity and drag coefficient captures both effects. In order to calculate the equivalent force as defined above, one has to know the particle's friction coefficient, $\xi(z_q)$. The friction coefficient is the ratio of force and the velocity as a function of the distance to the surface. $\xi(z_q)$ is obtained in still another FEM calculation using the same geometry, where a known external force, F, is applied to the particle. The friction coefficient is equal to $F/v(z_q)$, where the velocity $v(z_q)$ is calculated using the finite-element model. Since the calculation occurs in two dimensions, the product of the friction coefficient, $\xi(z_q)$, and the velocity, v_P, has units of N/m. The conversion to a 3D force in units of Newton is achieved by multiplication with the diameter of the particle. Evidently, the thus-derived force pertains to a section of an infinite cylinder with a length equal to the cylinder diameter. The force onto a sphere differs and this difference must be kept in mind.

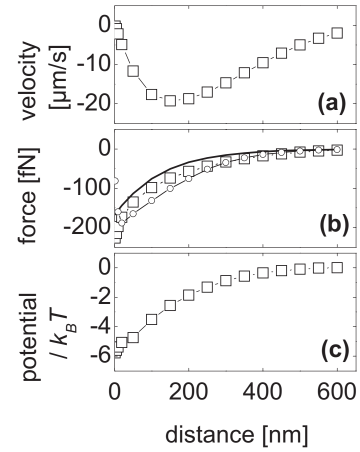

FIG. 3. Particle velocity (a), equivalent steady force (squares, b), time-averaged advected momentum integrated over the particle volume (small circles, b), and equivalent potential (c) obtained from the finite element calculation [cf. Fig. 2(c)]. The parameters were $u_{q,0} = 10$ nm, $R = 100$ nm, $\rho_{\text{liq}} = \rho_P = 1$ g/cm^3, $\eta = 1$ mPa s. The particle was rigid. The solid line in panel (b) is the prediction from Eq. (8).

Figures 3(b) shows the equivalent steady force ($F_S = \xi v_P$, squares) and the volume-integral of the time-averaged momentum (small circles). The two are similar, but not the same. Figure 3(c) shows the potential ($V_S(z_q)$) derived from the equivalent force versus distance, z_q. The potential was calculated by integrating the equivalent force from infinity to the respective distance [where $V_S(\infty) = 0$ by definition]. Clearly, the equivalent force and the potential decrease with distance from the surface and they do so in a roughly exponential manner. The range of the steady force is about 125 nm, which is half the thickness of the boundary layer [cf. Eq. (9)]. For the chosen conditions, V_S is of the order of the thermal energy, k_BT.

The data shown in Fig. 3 pertain to rigid particles. Being numerical, the calculation is readily extended to soft particles and droplets. An example of a steady flow field around a droplet is shown in Fig. 2(d). The numerical calculation predicts the total force as well as the droplet's deformation. Figure 4 shows force-distance curves obtained for droplets with varied viscosity, η_d. The droplets were assumed to be purely viscous ($G'_d = 0$, $G''_d = i\omega\eta_d$ with G_d the shear modulus of the droplet). For the sake of this particular argument, we neglected surface tension. For a more realistic calculation, surface tension should be included [35]. The viscosity of the droplet, η_d, was incremented logarithmically between 0.1 and 100 mPa s. The viscosity of the ambient liquid was maintained fixed at $\eta = 1$ mPa s. Interestingly, the steady force is *repulsive* for droplets, which are less viscous than the ambient liquid. An example would be droplets of water in oil. The force is directed *away from* the surface for $\eta_d < \eta$, which is the analog of buoyancy. Again, there is a caveat because of surface tension.

IV. STEADY FORCE ONTO A RIGID PARTICLE SET IN MOTION BY A TRANSVERSE VISCOUS WAVE

The numerical results shown in Fig. 3 suggest that there might be a set of approximations, which lead to a simple

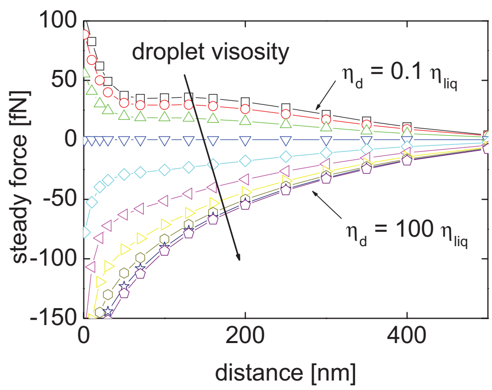

FIG. 4. (Color online) Force-distance curves computed for droplets of variable viscosity. The viscosity of the ambient liquid was 1 mPa s. The droplet radius was $R = 100$ nm. The viscosity of the droplet, η_d, was incremented logarithmically (3 steps/decade) from 0.1 mPa s to 100 mPa s.

analytical relation. We expect the potential, $V_S(z_q)$, to be exponential with a decay depth equal to about half the thickness of the boundary layer. In the following, we make such approximations. These are the following:

(a) The particle is rigid.

(b) The body force [the integral of the source term from Eq. (2) over the particle volume] is large compared to the contact force exerted by the adjacent liquid. Remember: we cannot integrate the stress tensor over a surface outside the Stokes layer because such a surface does not exist (cf. Sec. II).

(c) The particle follows the motion of the background fluid.

The third approximation is separate from the first and the second. It will only be invoked from Eq. (6) onward.

For a rigid particle the velocity field inside the particle is given as

$$\mathbf{v}_u(\mathbf{r},t) = \mathbf{v}_{c,u}(t) + \Omega_u(t) \times \mathbf{r}, \tag{3}$$

where $\mathbf{v}_{c,u}$ is the velocity of the particle's center, Ω_u is the rotational velocity, $\mathbf{r}$ is the distance to the particle center, and $\mathbf{v}_{c,u}$ and Ω_u are first-order quantities like $\mathbf{v}_u$. Their determination relies on a solution of the linear problem of hydrodynamics [Eq. (1)].

We decompose the advected momentum acting onto the particle itself in the usual form as

$$\begin{aligned}\mathbf{F}_S &= \int_{\text{Volume}} \mathbf{f}_S d^3\mathbf{r} \\ &= -\int_{\text{Volume}} \rho \left\langle (\mathbf{v}_u \cdot \nabla)\,\mathbf{v}_u \right\rangle d^3\mathbf{r} \\ &= \int_{\text{Volume}} \rho \left\langle (\mathbf{v}_u \times (\nabla \times \mathbf{v}_u)) \right\rangle d^3\mathbf{r} - \int_{\text{Volume}} \rho \left\langle \frac{1}{2}\nabla \mathbf{v}_u^2 \right\rangle d^3\mathbf{r},\end{aligned} \tag{4}$$

where $\mathbf{F}_S$ is a force in newtons. The second term in line 3 is zero for reasons of symmetry. The geometry does not have a polar axis. (This statement only concerns the particle itself, not the liquid around it.) Integration of the first term over the particle volume yields

$$\mathbf{F}_S = M \left\langle \mathbf{v}_c(t) \times \Omega(t) \right\rangle = -\frac{M}{2}\mathrm{Re}\left(\Omega_0^* \times \mathbf{v}_{c,0}\right), \tag{5}$$

where $M = \rho V$ is the particle's mass with V the particle volume.

Equation (5) looks as though it describes a Magnus force and one might view $\mathbf{F}_S$ as a time-averaged Magnus force [36–39]. Note, however, that *any* steady force acting onto the particle must contain a term of the form $\Omega \times \mathbf{v}$ for reasons of symmetry. The conventional Magnus force acts onto a body moving steadily relative to an inviscid fluid. The force is generated by the boundary layer. Here, the movement is oscillatory and the particle is coupled viscously to a nearby wall, which oscillates, as well. When portraying $\mathbf{F}_S$ as the conventional Magnus force, one misses an essential element of the problem.

Equation (5) holds for all rigid particles. In a second step, we make an approximation with regard to $\mathbf{v}_{c,0}$ and Ω_0, assuming that the particle diameter is much less than the thickness of the boundary layer. If this is the case, the particle (approximately) follows the movement of the background fluid. The flow field of the background fluid is entirely along the tangential direction (x). The velocity, $v_x(z,t)$ is given as

$$\begin{aligned}\mathrm{v}_x(z,t) &= \mathrm{Re}(\mathrm{v}_{x,0}(z)\exp(i\omega t)) = \mathrm{Re}(v_{q,0}\exp(i(\omega t - kz))) \\ &= \mathrm{Re}\left(\mathrm{v}_{q,0}\exp\left(i\left(\omega t - \frac{1-i}{\delta}z\right)\right)\right),\end{aligned} \tag{6}$$

where z is the distance to the surface and k is the complex-valued wave vector, pointing normal to the surface. One has $k = \omega(\rho/(i\omega\eta))^{1/2} = (1-i)/\delta$ with δ the depth of penetration of the transverse viscous wave ($\delta \sim 250$ nm at $\omega/2\pi = 5$ MHz in water). $\mathrm{v}_{x,0}(z)$ is the complex amplitude of the velocity and $\mathrm{v}_{q,0}$ is the amplitude at $z = 0$. $\mathrm{v}_{q,0}$ is equal to $i\omega u_{q,0}$, with $u_{q,0}$ the oscillation amplitude at the resonator surface. The amplitude was a few nanometers in Ref. [17].

The velocity gradient tensor of a transverse viscous wave can formally be decomposed into a symmetric and an antisymmetric part as $dv_x/dz = \frac{1}{2}(dv_x/dz + dv_z/dx) + \frac{1}{2}(dv_x/dz - dv_z/dx)$. The first term and the second term are the strain rate tensor and the rotation tensor, respectively. Since the particle is rigid, it only takes part in the rotation. If the particle is small, its rotation follows the rotation of the background fluid, evaluated at the position of the particle's center. The axis of rotation is the y axis. We have

$$\begin{aligned}\Omega_{y,0}(z) &= \frac{1}{2}\left(\frac{dv_{x,0}(z)}{dz} - \frac{dv_{z,0}(z)}{dx}\right) \\ &= \frac{1}{2}\frac{dv_{x,0}(z)}{dz} = -\frac{ik}{2}\mathrm{v}_{x,0}(z).\end{aligned} \tag{7}$$

In step 2, we used $v_z \equiv 0$ for the background fluid. z is the position of the center of the particle. There is a phase shift between translation and rotation because the wave vector, k, is complex. Equation (7) can also be obtained from Eq. 4.18 in Ref. [40] with the particle being buoyancy-matched and with small ω. The limit of $\omega \to 0$ is appropriate because we have assumed the particle radius to be much smaller than $\delta = (2\eta/(\rho\omega))^{1/2}$. Inserting Eq. (6) and Eq. (7) into Eq. (5)

one finds

$$\begin{aligned}\mathbf{F}_S &= -\frac{M}{2}\mathrm{Re}\left(\Omega_0^* \times \mathbf{v}_{c,0}\right)\\ &= \frac{M}{2}\mathrm{Re}\left(\frac{ik^*}{2}v_{x,0}^*(z)\,v_{x,0}(z)\right)\hat{\mathbf{z}}\\ &= \frac{M}{2}\mathrm{Re}\left(\frac{i-1}{2\delta}\left|v_{x,0}(z)\right|^2\right)\hat{\mathbf{z}}\\ &= -\frac{M}{4\delta}\left|v_{q,0}^2\right|\exp\left(-\frac{2z}{\delta}\right)\hat{\mathbf{z}}\\ &= -\frac{M}{4\delta}\omega^2\left|u_{q,0}^2\right|\exp\left(-\frac{2z}{\delta}\right)\hat{\mathbf{z}},\end{aligned} \quad (8)$$

$\hat{\mathbf{z}}$ is the unit vector along z. Clearly, there is an attractive force, decaying exponentially with distance. The solid line in Fig. 3(b) is the prediction from Eq. (8). It reproduces the numerical result rather well.

Since the $\mathbf{F}_S(\mathbf{r})$ has vanishing curl, one can define a potential as

$$V_S = \int_\infty^z -\mathbf{F}_S(z')\,d\mathbf{z}' = -\frac{M}{8}\omega^2\left|u_{q,0}^2\right|\exp\left(-\frac{2z}{\delta}\right). \quad (9)$$

The potential at infinity was set to zero. From the comparison of V_S to the thermal energy, k_BT, one can assess whether the steady force is strong enough to overcome Brownian motion. Inserting the experimental values from Ref. [17] ($R = 100$ nm, $\rho = 1$ g/cm^3, $u_{q,0} = 10$ nm, $\omega = 2\pi$ 5 MHz) and $z \approx 2R$, one finds a potential of 2.5 k_BT. An attractive force of this magnitude is relevant to experiment. It is strong enough to overcome Brownian motion and, also, to compete with other surface forces, for instance induced by electrostatic repulsion.

V. DROPLETS WITH A DENSITY DIFFERING FROM THE DENSITY OF THE AMBIENT FLUID

Above we have chosen the density constant throughout the entire volume. If we allow for variable density, the advected momentum term of the Navier-Stokes equation acquires a component proportional to the gradient in density,

$$\mathbf{f}_S = -\langle(\mathbf{v}_u\cdot\nabla)\rho\mathbf{v}_u\rangle = -\rho\langle(\mathbf{v}_u\cdot\nabla)\mathbf{v}_u\rangle + -\mathbf{v}_u\langle(\mathbf{v}_u\cdot\nabla\rho)\rangle. \quad (10)$$

At an interface with a discontinuity in ρ, the gradient in density turns into a δ function,

$$\nabla\rho = \left(\rho_{\mathrm{bulk}} - \rho_{\mathrm{droplet}}\right)\ \delta(\mathbf{r} - \mathbf{R}_S)\,\hat{\mathbf{n}}, \quad (11)$$

where $\hat{\mathbf{n}}$ is the unit vector along the surface normal and $\mathbf{R}_S$ is a location at the interface. $\delta(r - R_S)$ is meant to integrate to unity, when the integration path is along the surface normal. Clearly, the steady force contains a contribution from the interface. As long as one is only concerned with rigid particles, one can avoid explicit treatment of the interface term by integrating the force density as

$$\begin{aligned}\mathbf{F}_S &= \int_{\mathrm{Volume}} \mathbf{f}_S d^3\mathbf{r} = -\int_{\mathrm{Volume}} \nabla\cdot\sigma_S d^3\mathbf{r}\\ &= -\int_{\mathrm{Surface}} \mathbf{n}\cdot\sigma_S d^2\mathbf{r}_S.\end{aligned} \quad (12)$$

Step 2 makes use of the fact the force density is the divergence of the stress tensor. σ_S is the Reynolds stress. One has $\sigma_{S,ij} = \rho\,\mathbf{v}_i\mathbf{v}_j$. Gauss's theorem was applied in step 3. The integral contains a contribution from the bulk (proportional the density inside the particle) and a contribution from the interface (proportional to the density mismatch). These two terms partially cancel each other. However, there is no need to explicitly account for the interface term, because one might as well integrate $\rho_{\mathrm{liq}}\mathbf{v}_i\mathbf{v}_j$ over an area just outside of the interface. This integral yields a term similar to Eq. (6), but the prefactor contains the density of the liquid (because the integration occurs inside the liquid). The body force onto the particle (including the interface term but not the contact forces exerted by the adjacent liquid) is

$$\mathbf{F}_S = \rho_{\mathrm{liq}}V_P\,\langle\mathbf{v}_c(t)\times\Omega(t)\rangle = -\frac{\rho_{\mathrm{liq}}V_P}{2}\mathrm{Re}\left(\Omega_0^*\times\mathbf{v}_{c,0}\right). \quad (13)$$

The mass of the particle in Eq. (6) has to be replaced by the product of the particle's volume and the density of the liquid.

However, this argument does not apply if one aims at the deformation of a droplet. Droplets experience displacement as well as deformation. For the calculation of the deformation, the steady force field inside the particle is needed and the interface term must be taken into account.

VI. SUMMARY

Colloidal particles located closely above a solid surface launching acoustic transverse viscous waves are attracted towards this surface. For an oscillation amplitude of 10 nm and a particle size of 100 nm, the force is strong enough to overcome Brownian motion. For liquid droplets, the direction of the force depends on the ratio of the droplets viscosity to the viscosity of the liquid. If the droplet is less viscous than the ambient medium, it repelled from the surface. This is analogous to buoyancy.

ACKNOWLEDGMENT

We thank Stefan Rosenthal for helpful discussions.

[1] Lord Rayleigh, Philos. Trans. R. Soc. London A **175**, 1 (1883).
[2] S. B. Pope, *Turbulent Flows* (Cambridge University Press, Cambridge, UK, 2000).
[3] C. S. Zhang, D. Xing, and Y. Y. Li, Biotechnol. Adv. **25**, 483 (2007).
[4] A. Wixforth, C. Strobl, C. Gauer, A. Toegl, J. Scriba, and Z. von Guttenberg, Anal. Bioanal. Chem. **379**, 982 (2004).
[5] J. Friend and L.Y. Yeo, Rev. Mod. Phys. **83**, 647 (2011).
[6] G. Yu, X. L. Chen, and J. Xu, Soft Matter **7**, 10063 (2011).

[7] F. Petersson, A. Nilsson, C. Holm, H. Jonsson, and T. Laurell, Analyst **129**, 938 (2004).
[8] L. A. Kuznetsova and W. T. Coakley, Biosens. Bioelectron. **22**, 1567 (2007).
[9] L. Sandrin, B. Fourquet, J. M. Hasquenoph, S. Yon, C. Fournier, F. Mal, C. Christidis, M. Ziol, B. Poulet, F. Kazemi, M. Beaugrand, and R. Palau, Ultrasound Med. Biol. **29**, 1705 (2003).
[10] Q. Qi and G. J. Brereton, IEEE Trans. Ultrason. Ferroelectr. Freq. Control **42**, 619 (1995).
[11] M. O. Lamminen, H. W. Walker, and L. K. Weavers, J. Membr. Sci. **237**, 213 (2004).
[12] M. Pohl, S. Hogekamp, N. Q. Hoffmann, and H. P. Schuchmann, Chemie Ingenieur Technik **76**, 392 (2004).
[13] J. Lighthill, J. Sound Vib. **61**, 391 (1978).
[14] N. Riley, Theor. Comput. Fluid Dyn. **10**, 349 (1998).
[15] N. Riley, Annu. Rev. Fluid Mech. **33**, 43 (2001).
[16] H. Bruus, J. Dual, J. Hawkes, M. Hill, T. Laurell, J. Nilsson, S. Radel, S. Sadhal, and M. Wiklund, Lab on a Chip **11**, 3579 (2012).
[17] M. Edvardsson, M. Rodahl, and F. Hook, Analyst **131**, 822 (2006).
[18] V. Heitmann and J. Wegener, Anal. Chem. **79**, 3392 (2007).
[19] C. Steinem and A. Janshoff, *Piezoeletric Sensors* (Springer, Heidelberg, 2006).
[20] M. A. Cooper, F. N. Dultsev, T. Minson, V. P. Ostanin, C. Abell, and D. Klenerman, Nat. Biotechnol. **19**, 833 (2001).
[21] Z. X. Lin and M. D. Ward, Anal. Chem. **67**, 685 (1995).
[22] C. Y. Wang and B. Drachman, Appl. Sci. Res. **39**, 55 (1982).
[23] S. S. Sadhal, Lab on a Chip **12**, 2292 (2012).
[24] R. König and D. Johannsmann (unpublished).
[25] R. Q. Liang, D. Liang, F. S. Yan, Z. Q. Liao, and G. D. Duan, Microgravity Sci. Technol. **23**, 79 (2011).
[26] M. Saadatmand and M. Kawaji, Microgravity Sci. Technol. **22**, 433 (2010).
[27] M. Saadatmand, M. Kawaji, and H. H. Hu, Microgravity Sci. Technol. **24**, 53 (2012).
[28] L. P. Gor'kov, Sov. Phys. Dokl. **1062**, 6 (1961).
[29] L. V. King, Proc. R. Soc. London A **147**, 212 (1934).
[30] H. Bruus, Lab on a Chip **12**, 20 (2012).
[31] K. Yosioka and Y. Kawasima, Acoustica **5** (1955).
[32] M. Settnes and H. Bruus, Phys. Rev. E **85**, 016327 (2012).
[33] D. Johannsmann, I. Reviakine, E. Rojas, and M. Gallego, Anal. Chem. **80**, 8891 (2008).
[34] D. Johannsmann, I. Reviakine, and R. P. Richter, Anal. Chem. **81**, 8167 (2009).
[35] A. A. Doinikov and A. Bouakaz, J. Acoust. Soc. Am. **127**, 703 (2010).
[36] G. K. Batchelor, *An Introduction to Fluid Dynamics* (Cambridge University Press, Cambridge, UK, 1967).
[37] P. G. Saffman, J. Fluid Mech. **22**, 385 (1965).
[38] S. I. Rubinow and J. B. Keller, J. Fluid Mech. **11**, 447 (1961).
[39] R. Kurose and S. Komori, J. Fluid Mech. **384**, 183 (1999).
[40] B. U. Felderhof, Physica A **166**, 492 (1990).